

Supplementary Information

The repurposed drugs Suramin and Quinacrine cooperatively inhibit SARS-CoV-2 3CL^{pro} *in vitro*

Raphael J. Eberle^{1,2#*}, Danilo S. Olivier³, Marcos S. Amaral⁴, Ian Gering¹, Dieter Willbold^{1,2,5}, Raghuvir K. Arni⁶, Monika A. Coronado^{1,6#*}

¹Institute of Biological Information Processing (IBI-7: Structural Biochemistry), Forschungszentrum Jülich, Jülich, Germany.

²Institut für Physikalische Biologie, Heinrich-Heine-Universität Düsseldorf, Universitätsstraße, Düsseldorf, Germany.

³Federal University of Tocantins, Araguaína-TO, Brazil.

⁴Institute of Physics, Federal University of Mato Grosso do Sul, Campo Grande-MS, Brazil.

⁵JuStruct: Jülich Centre for Structural Biology, Forschungszentrum Jülich, Jülich, Germany.

⁶Multiuser Center for Biomolecular Innovation, IBILCE, Universidade Estadual Paulista (UNESP), São Jose do Rio Preto-SP, Brazil.

#both authors contributed equally

*Correspondence to eberleraphael@gmail.com or monikacoronado@gmail.com

Table of contents

Supplementary Figure S1. Purification of SARS-Cov-2 3CL^{pro} and quality check of the produced protein.

Supplementary Figure S2. K_M determination of SARS-CoV-2 3CL^{pro}.

Supplementary Figure S3. Effect of Triton X-100 on the Quinacrine and Suramin inhibition against 3CL^{pro}.

Supplementary Figure S4. H₂O₂ generating capacity of Quinacrine and Suramin under the influence of 1mM TCEP.

Supplementary Figure S5. Quinacrine and Suramin with inhibitory activity against SARS-CoV-2 3CL^{pro}.

Supplementary Figure S6. Fluorescence spectroscopy of Trp at 295 nm of SARS-CoV-2 3CL^{pro} in the presence of the Suramin and Quinacrine.

Supplementary Figure S7. K_D determination of Quinacrine binding to SARS-CoV-2 3CL^{pro} using SPR.

Supplementary Figure S8. K_D determination of Suramin binding to SARS-CoV-2 3CL^{pro} using SPR.

Supplementary Figure S9. K_D determination of Quinacrine binding to SARS-CoV-2 3CL^{pro} under the influence of Suramin using SPR.

Supplementary Figure S10. Clustering analysis of the SARS-CoV-2 3CL^{pro} structure after MD simulation.

Supplementary Figure S11. Time dependent modifications of the SARS-CoV-2 3CL^{pro} dimer.

Supplementary Figure S12. SARS-CoV-2 3CL^{pro} dimeric structure after MD simulation.

Supplementary Figure S13. Time dependent modifications of SARS-CoV-2 3CL^{pro} dimer in the presence of Quinacrine in each active site.

Supplementary Figure S14. Time dependent modifications of SARS-CoV-2 3CL^{pro} dimer in the presence of Suramin. Supplementary Figure S15. Atom numbers of Quinacrine and Suramin.

Supplementary Figure S16. Quinacrine and Suramin combination with inhibitory activity against SARS-CoV-2 3CL^{pro}.

Supplementary Figure S17. Time dependent modifications of SARS-CoV-2 3CL^{pro} dimer in the presence of Quinacrine and Suramin.

Table S1. K_D values of Quinacrine and Suramin SARS-CoV-2 3CL^{pro}, determined by SPR.

Table S2. Contributing amino acids in the substrate-binding sites of SARS-CoV-2 3CL^{pro}.

Table S3. SARS-CoV-2 3CL^{pro} Residues involved in forming H-bonds and hydrophobic contacts with Quinacrine, Suramin and Quinacrine + Suramin.

Table S4. Affected proteins by mutations in SARS-CoV-2 variants.

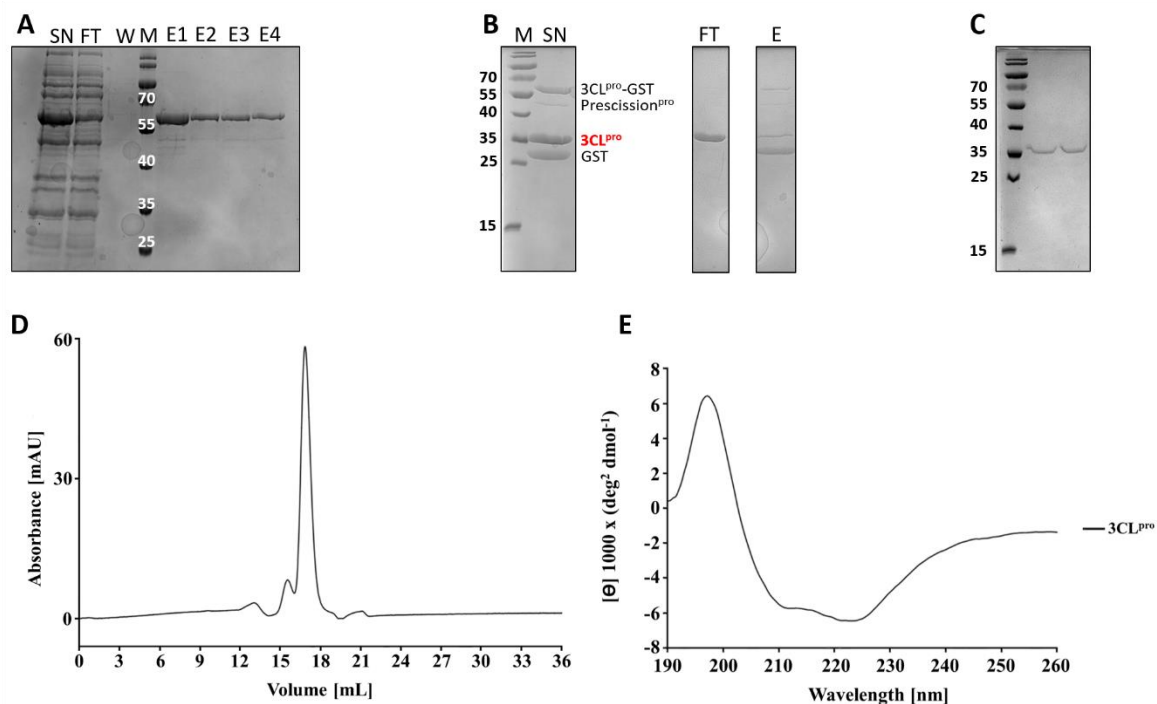


Figure S1. Purification of SARS-Cov-2 3CL^{pro} and quality check of the produced protein. (A) SDS 15% Gel of 3CL^{pro}-GST purification with GSH sepharose. SN: supernatant, FT: flow through, W: washing step, M: protein marker, E1-E4: Elution. (B) SDS 15% Gel of the 3CL^{pro}-GST fusion protein cleavage by PreScission^{pro}. M: protein marker. SN: cleaving approach, containing 3CL^{pro}-GST, PreScission^{pro}, 3CL^{pro} and GST. FT: contain 3CL^{pro}, E: elution contains uncleaved 3CL^{pro}-GST, PreScission^{pro} and GST. (C) SDS 15% Gel of 3CL^{pro} after size exclusion chromatography. (D) 3CL^{pro} Chromatogram after size exclusion chromatography. (E) CD spectrum of 3CL^{pro}.

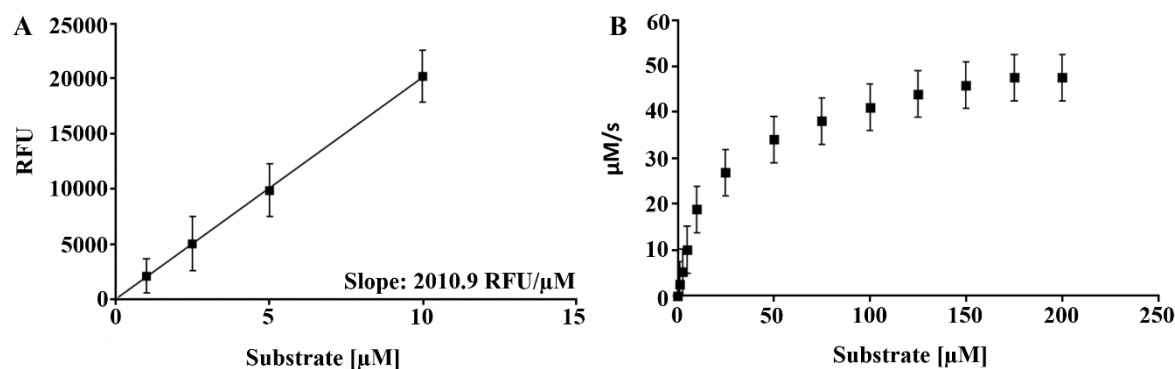


Figure S2. K_M determination of SARS-CoV-2 3CL^{pro}. (A) Standard curve to convert RFU to the amount of the cleaved substrate (μM). (B) Michaelis-Menten plot of 0.5 μM protein with various concentrations of FRET substrate. Curve fitting with Michaelis-Menten equation gave the best fitting values of K_M and V_{max} as 25.47 ± 3.43 μM and 47.52 ± 2.91 μM/s, respectively. Data shown are the mean ± SD from three independent measurements (n=3).

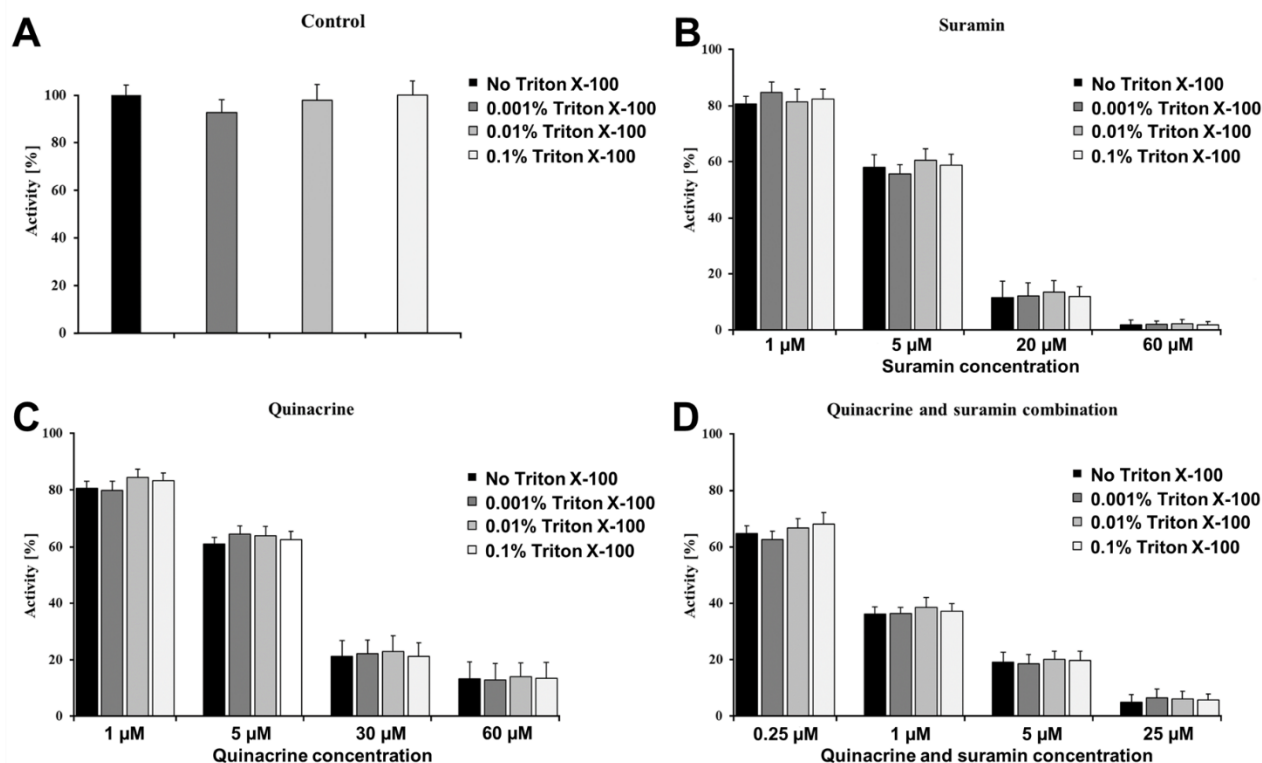


Figure S3. Effect of Triton X-100 on the Quinacrine and Suramin inhibition against SARS-CoV-2 3CL^{pro}. The experiments were performed to exclude the possibility that the molecules inhibit the protease promiscuously by aggregation. Three Triton X-100 concentrations (0.001%, 0.01% and 0.1%) were tested with four different inhibitor concentrations and compared with the results without detergent. Additionally, the effect of Triton X-100 against the protease was tested. Data shown are the mean \pm SD from three independent measurements (n=3). **(A)** Effect of Triton X-100 on 3CL^{pro} activity. **(B)** Effect of Triton X-100 on Suramin inhibition against 3CL^{pro}. **(C)** Effect of Triton X-100 on Quinacrine inhibition against 3CL^{pro}. **(D)** Effect of Triton X-100 on Quinacrine and Suramin (combination) inhibition against 3CL^{pro}.

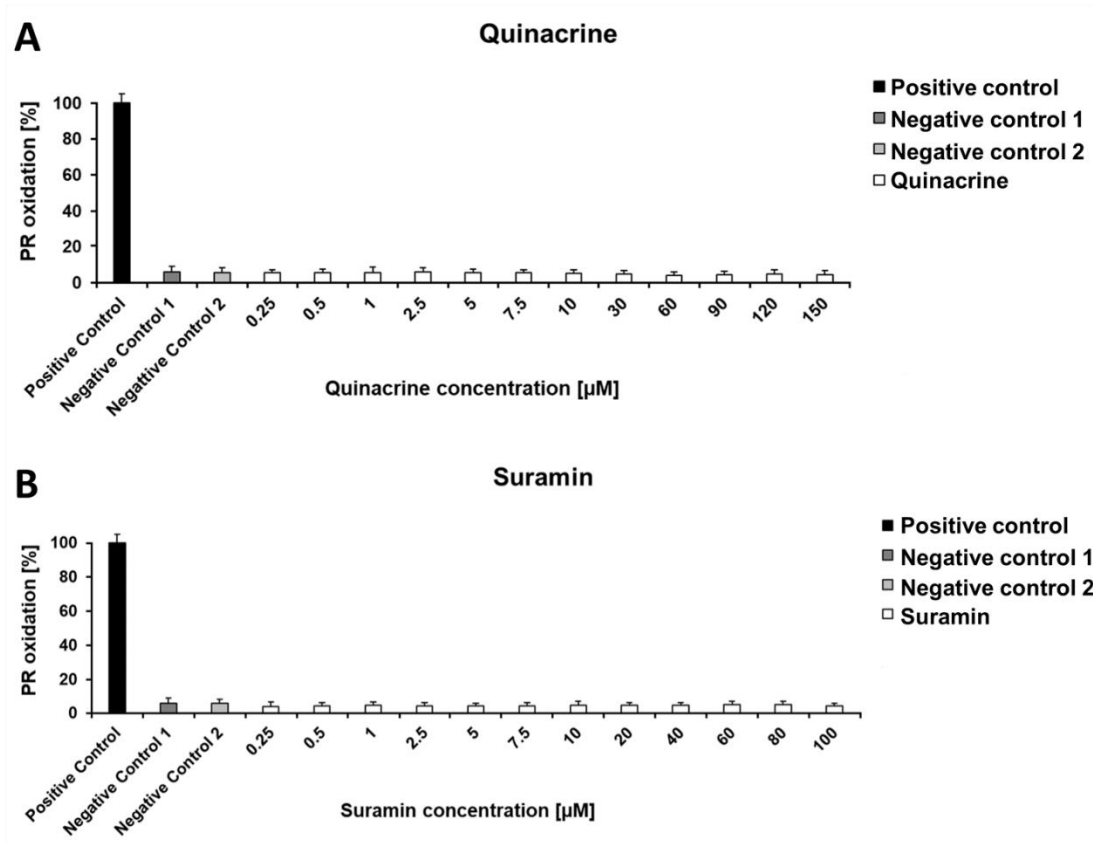


Figure S4. H₂O₂ generating capacity of Quinacrine and Suramin under the influence of 1mM TCEP. The experiments were performed to measure the H₂O₂ generating capacity of Quinacrine and Suramin under the influence of 1mM TCEP. Further, the H₂O₂-dependent horseradish peroxidase (HRP) mediates the oxidation of phenol red (PR), which can be followed at 610 nm. Positive control: HRP-PR and H₂O₂; negative control 1: HRP-PR; negative control 2: PR; Data showed are the mean \pm SD from three independent measurements (n=3). **(A)** H₂O₂ generation by Quinacrine. **(B)** H₂O₂ generation by Suramin.

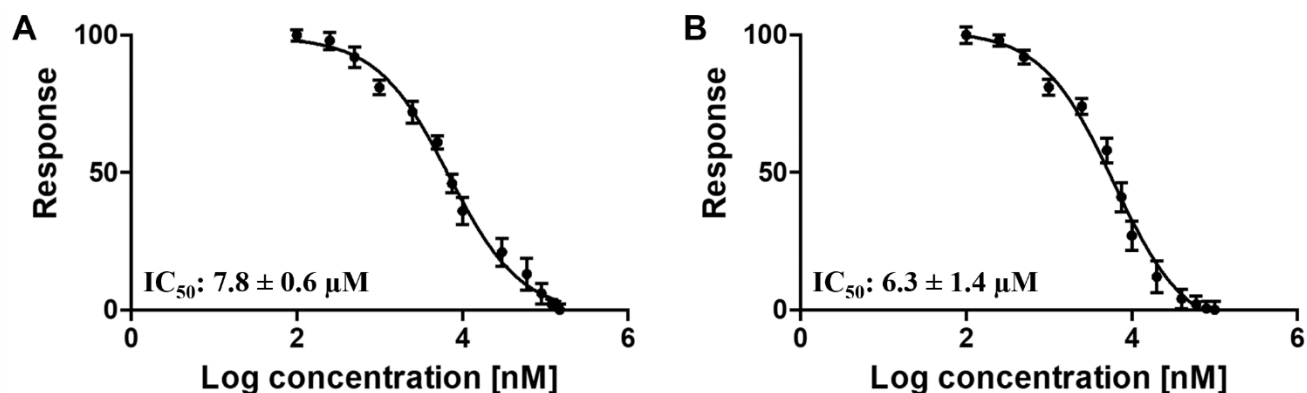


Figure S5. Quinacrine and Suramin with inhibitory activity against SARS-CoV-2 3CL^{pro}. Dose response curves for IC₅₀ determination. The normalized response [%] of SARS-CoV-2 3CL^{pro} is plotted against the Log of the Quinacrine and Suramin concentration. The determined IC₅₀ values are presented within the corresponding picture. (A) Dose response curve of Quinacrine and SARS-CoV-2 3CL^{pro}. (B) Dose response curve of Suramin and SARS-CoV-2 3CL^{pro}. Data shown are the mean \pm SD from three independent measurements (n=3).

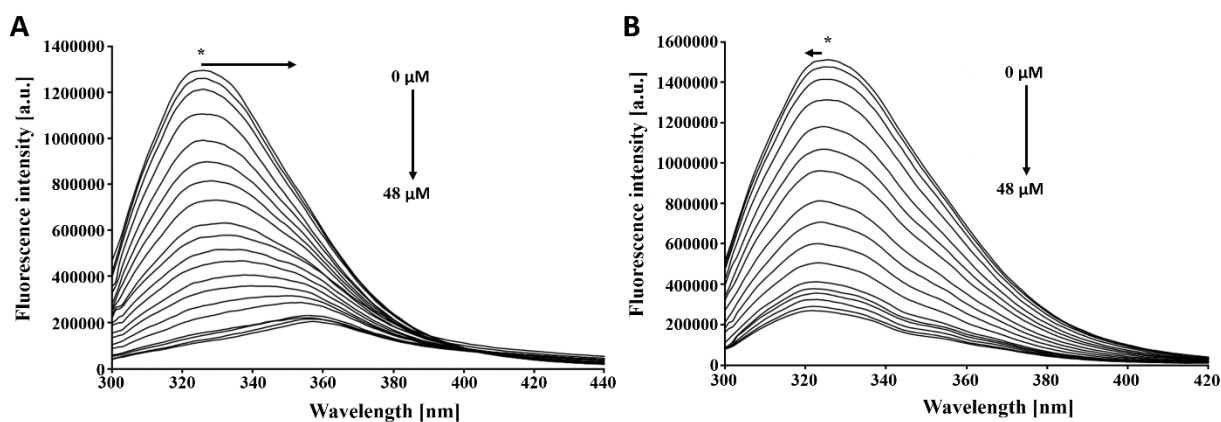


Figure S6. Fluorescence spectroscopy of Trp at 295 nm of SARS-CoV-2 3CL^{pro} in the presence of the Suramin and Quinacrine. (A) Fluorescence of SARS-CoV-2 3CL^{pro} under influence of Suramin titration demonstrated a red excitation shift of visible Trp (B) Fluorescence of SARS-CoV-2 3CL^{pro} under influence of Quinacrine titration demonstrated a blue excitation shift of visible Trp (*).

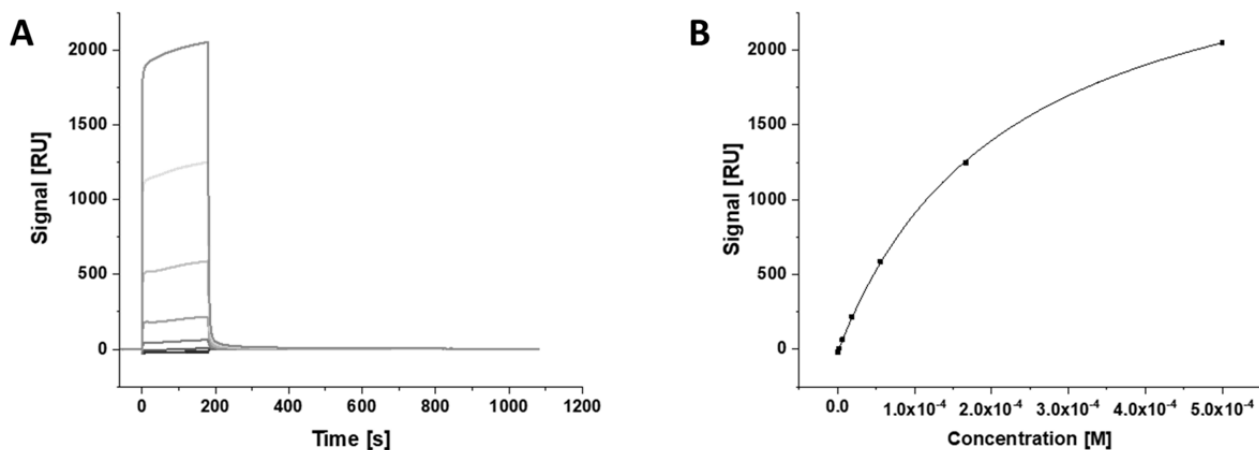


Figure S7. Equilibrium dissociation constant (K_D) determination of Quinacrine binding to SARS-CoV-2 3CL^{pro} using surface plasmon resonance (SPR). (A) SPR sensorgram of 3CL^{pro} and Quinacrine. (B) Saturation curve for the Quinacrine and 3CL^{pro} interaction.

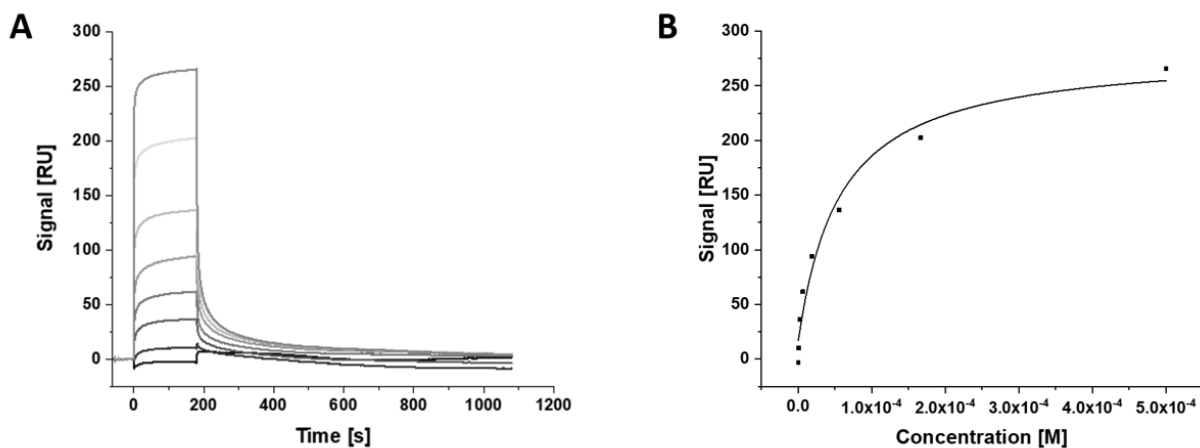


Figure S8. Equilibrium dissociation constant (K_D) determination of Suramin binding to SARS-CoV-2 3CL^{pro} using surface plasmon resonance (SPR). (A) SPR sensorgram of 3CL^{pro} and Suramin. (B) Saturation curve for the Suramin and 3CL^{pro} interaction.

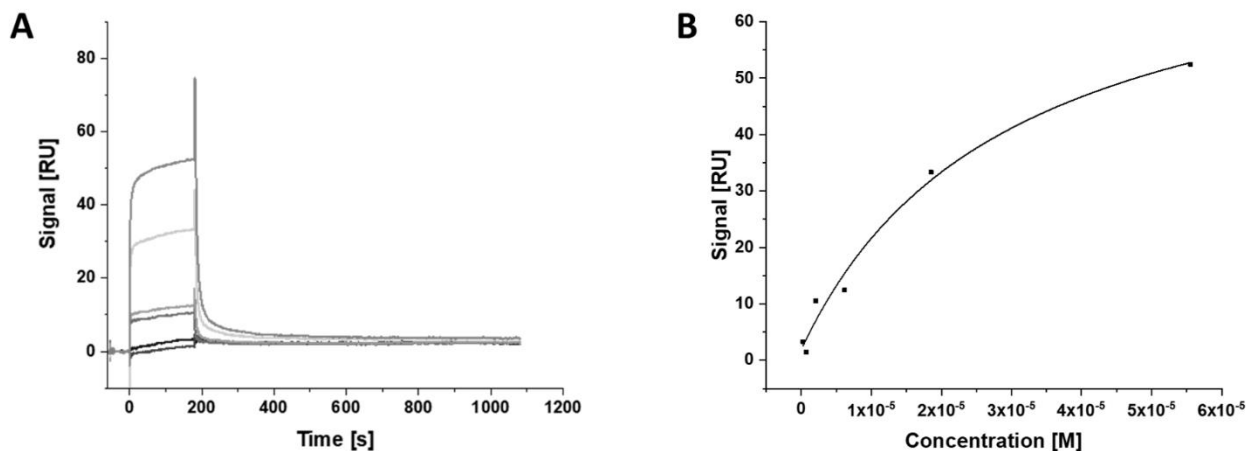


Figure S9. Equilibrium dissociation constant (K_D) determination of Quinacrine binding to SARS-CoV-2 3CL^{pro} under Suramin influence using surface plasmon resonance (SPR). (A) SPR sensorgram of 3CL^{pro} and Quinacrine under influence of Suramin. (B) Saturation curve for the Quinacrine and 3CL^{pro} interaction.

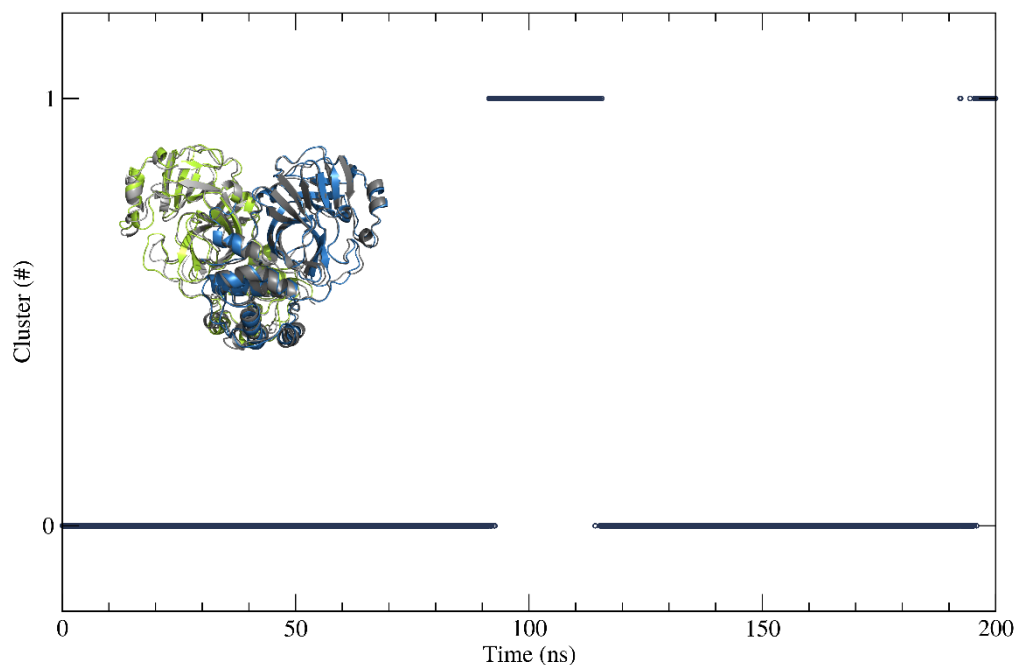


Figure S10. Clustering analysis of the SARS-CoV-2 3CL^{pro} structure after MD simulation. Pure protein pointed to a chosen structure (cluster 0) that was representative for over 86,1% of the simulation and appeared around 169 ns. The representative structure (C0) is in green and blue, while the (C1) is colored in grey.

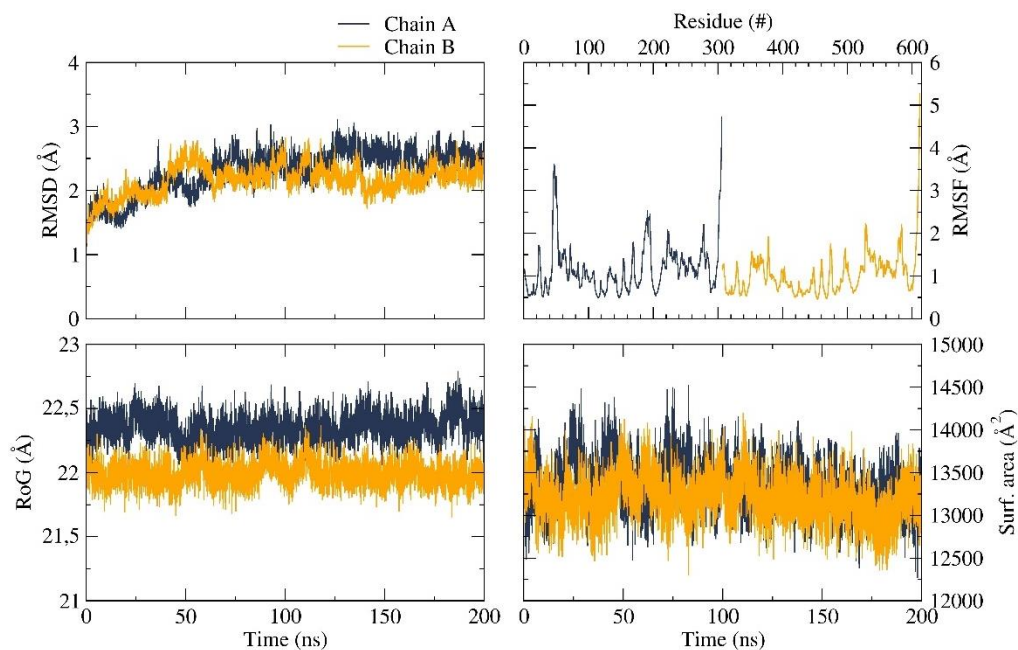


Figure S11. Time dependent modifications of the SARS-CoV-2 3CL^{pro} dimer. Protomer 1 (blue) and protomer 2 (yellow). RMSD, RoG and surface area as function of time. RMSF for each amino acid.

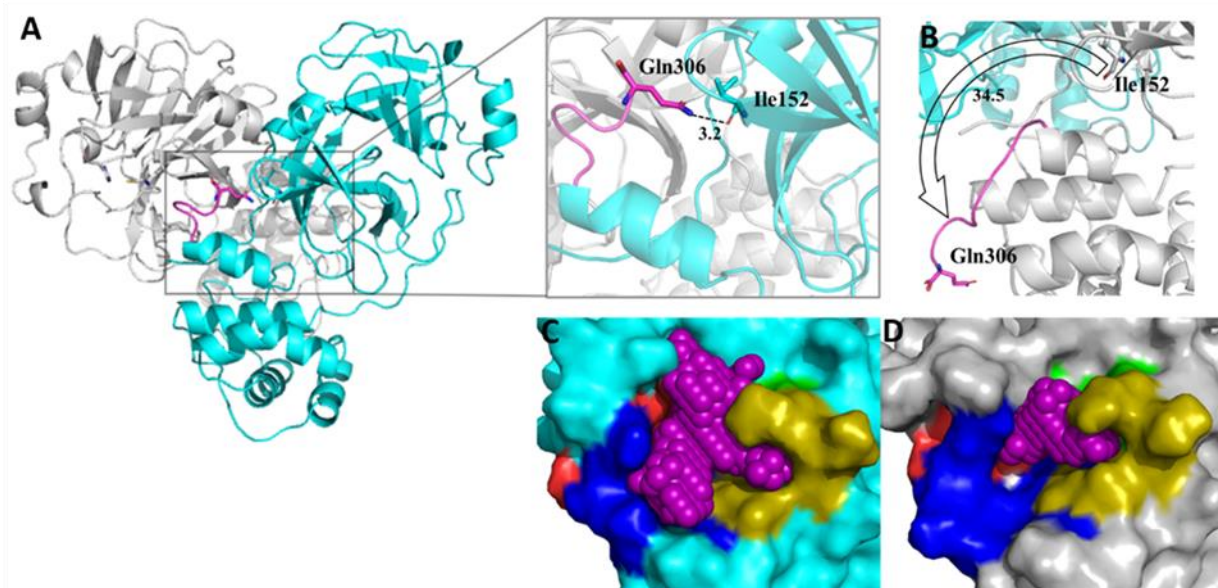


Figure S12. SARS-CoV-2 3CL^{PRO} dimeric structure after MD simulation. (A) SARS-CoV-2 3CL^{PRO} in ribbon view, protomer 1 in turquoise and protomer 2 in grey. H-bond between C-terminus Gln306 and Ile152 in protomer 1 is highlighted. (B) Protomer 2 Gln306 and Ile152 develop no H-bond. (C) Protomer 1 active site pocket volume yields around 261 Å³, the substrate binding subsites are highlighted. Green S1'; gold S1; red S2 and blue S3. (D) Protomer 2 active site volume yields about 142 Å³.

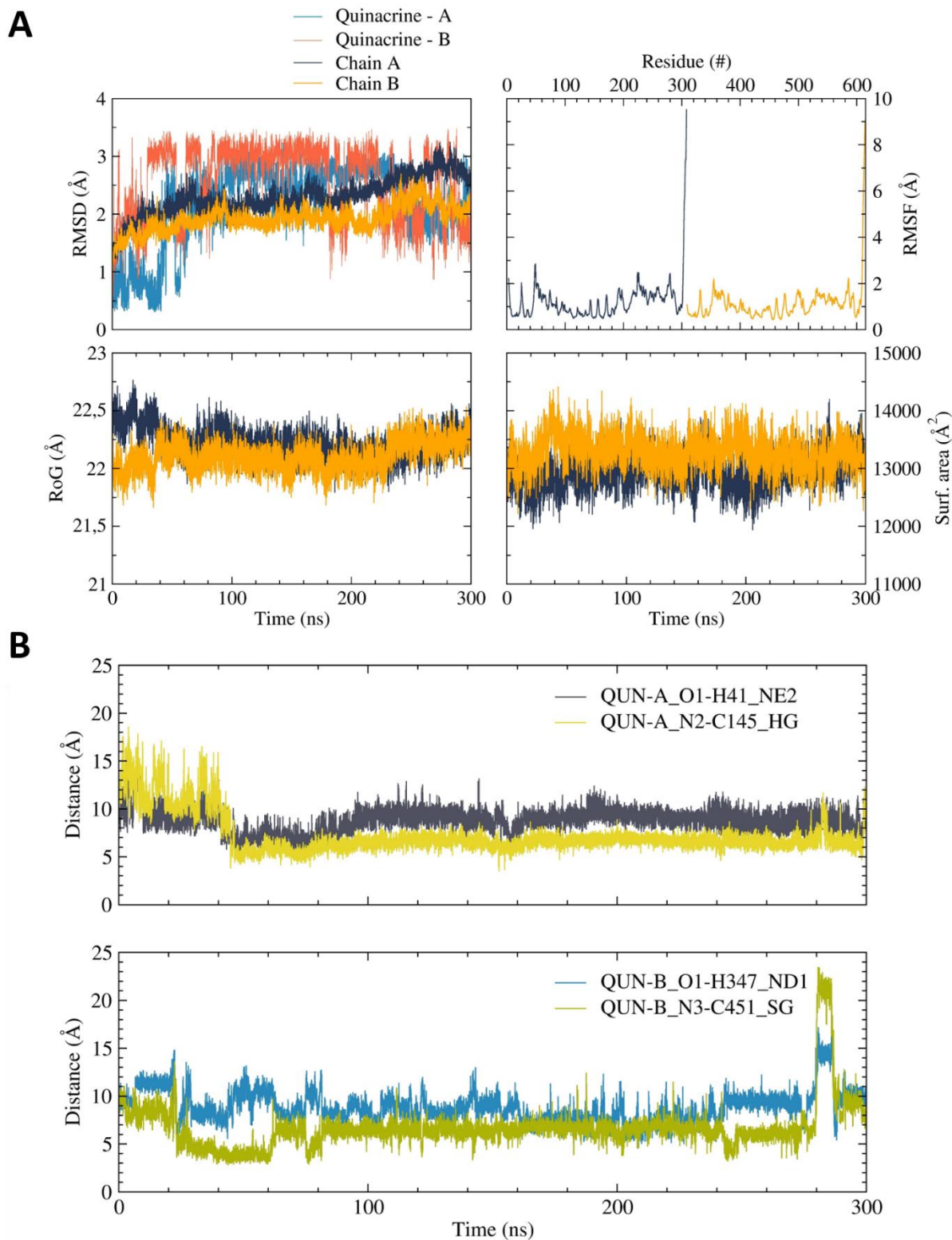


Figure S13. Time dependent modifications of SARS-CoV-2 3CL^{pro} dimer in the presence of Quinacrine in each active site. (A) Protomer 1 (blue), Quinacrine A (light blue), protomer 2 (yellow) and Quinacrine B (pink). RMSD, RoG and surface area as function of time. RMSF for each amino acid. **(B)** Distance over time of Quinacrine A and B in the protease active site.

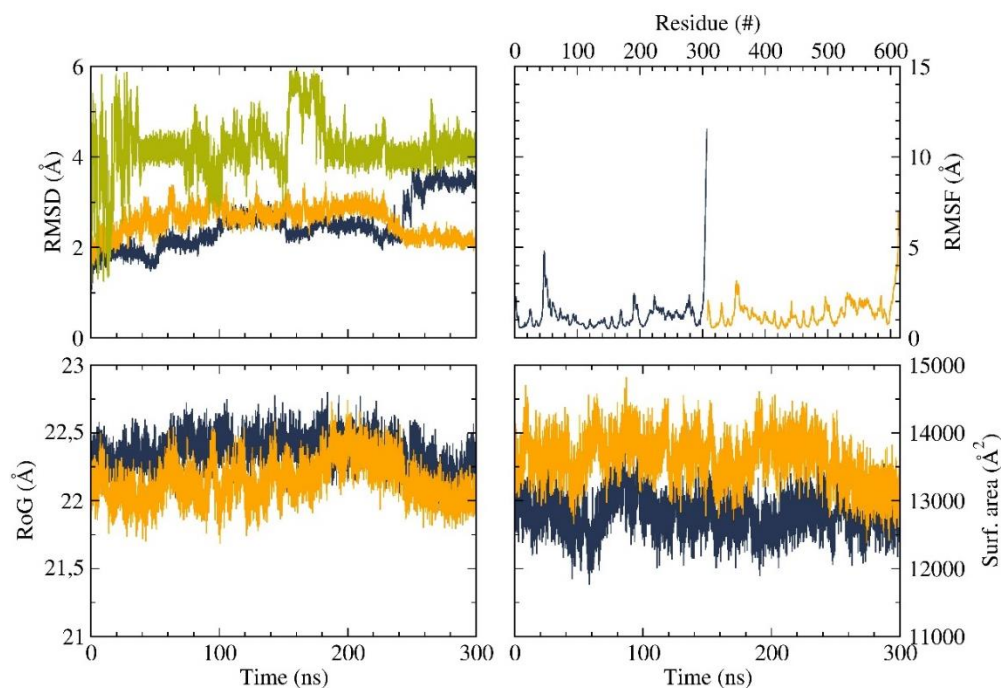


Figure S14. Time dependent modifications of SARS-CoV-2 3CL^{pro} dimer in the presence of Suramin. Protomer 1 (blue), protomer 2 (yellow) and Suramin (green). RMSD, RoG and surface area as function of time. RMSF for each amino acid.

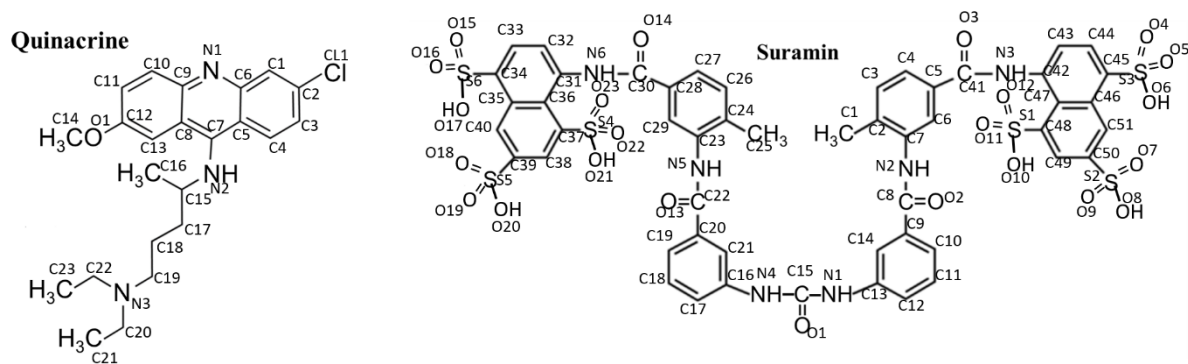


Figure S15. Atom numbers of Quinacrine and Suramin.

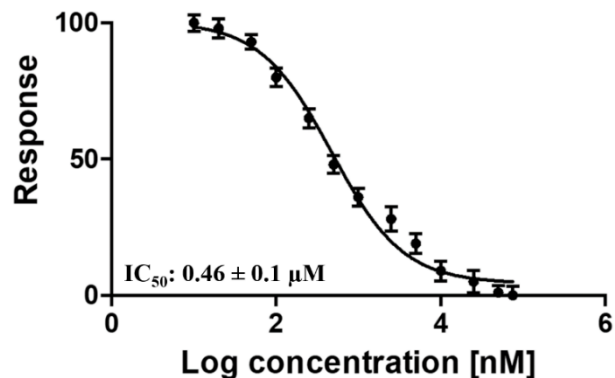


Figure S16. Quinacrine and Suramin combination with inhibitory activity against SARS-CoV-2 3CL^{pro}. Dose response curve for IC₅₀ determination. The normalized response [%] of SARS-CoV-2 3CL^{pro} is plotted against the Log of the combined Quinacrine and Suramin concentration. The determined IC₅₀ value is presented within the figure. Data shown are the mean ± SD from three independent measurements (n=3).

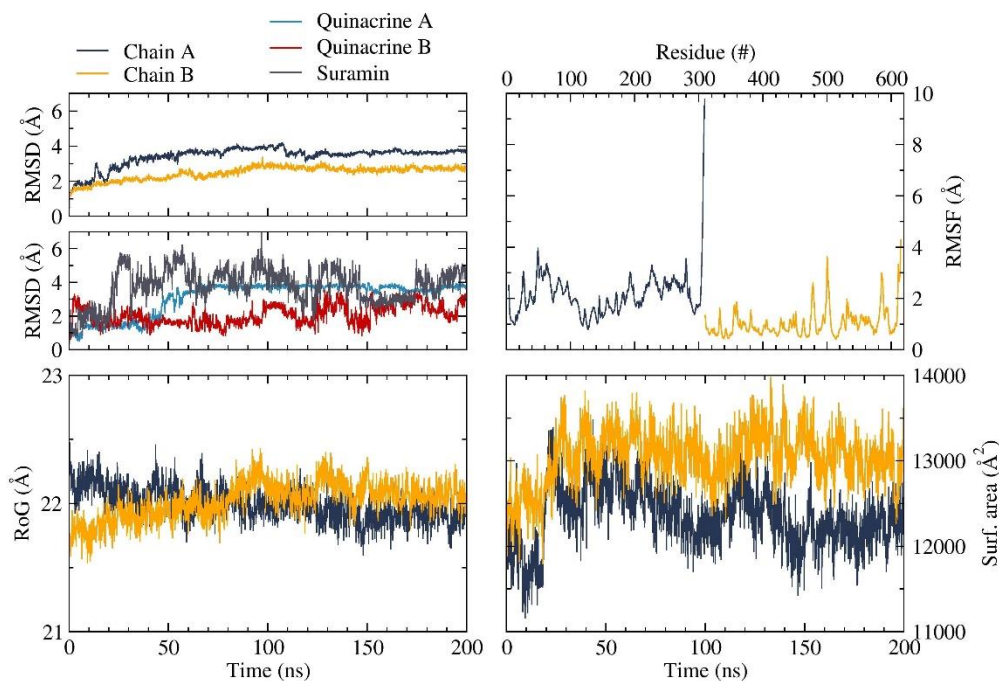


Figure S17. Time dependent modifications of SARS-CoV-2 3CL^{pro} dimer in the presence of Quinacrine and Suramin. Protomer 1 (blue), protomer 2 (yellow), Suramin (gray), Quinacrine A (light-blue), Quinacrine B (red). RMSD, RoG and surface area as function of time. RMSF for each amino acid.

Table S1. K_D values of Quinacrine and Suramin SARS-CoV-2 3CL^{pro}, determined by SPR.

Molecule	Experiment 1 K_D [μ M]	Experiment 2 K_D [μ M]	Experiment 3 K_D [μ M]	Average K_D [μ M]	STD [μ M]
Quinacrine	233.5	222.3	-	227.9	± 7.9
Suramin	62.9	56.5	-	59.7	± 4.5
Quinacrine*	15.05	45.9	29.6	30.2	± 12.7

* K_D determination of Quinacrine to SARS-CoV-2 3CL^{pro} in the presence of Suramin.

Table S2. Contributing amino acids in the Substrate-binding site of SARS-CoV-2 3CL^{pro}.

Substrate subsite*	SARS-CoV-2 3CL ^{pro}
S1'	<u>His41</u>
	Gly143
	Ser144
	<u>Cys145</u>
S1	Phe140
	Leu141
	Asn142
	His163
	Glu166
S2	<u>His41</u>
	Met49
	Tyr54
	His164
	Asp187
	Arg188
S3	Met165
	Glu166
	Leu167
	Gln189
	Thr190
	Gln192
Oxyanion hole	<u>His41</u>
	<u>Cys145</u>

* Based on Tang et al. 2020 [1]

Table S3. SARS-CoV-2 3CL^{pro} Residues involved in forming H-bonds and hydrophobic contacts with Quinacrine, Suramin and Quinacrine + Suramin.

Ligand	Interacting residues	
	H-Bond	Hydrophobic interaction
Quinacrine	Met165, Gln189	His41, Met49, Val186, Asp187, Arg188, Gln194
Suramin	Lys12, Lys97, Lys100, Tyr101, Phe103	Lys97, Lys100, Lys102, Phe103, Val104, Arg105
Quinacrine (+Suramin)	Thr45	Thr25, His41, Cys44, Thr45, Met49, Pro52
Suramin (+Quinacrine)	Lys12, Thr98, Lys97'	Pro96, Lys97, Thr98, Tyr 101

Table S4. Affected proteins by mutations in SARS-CoV-2 variants.

Variant	Origin	Orf1ab	Orf3	Orf8	S ¹	E ²	M ³	N ⁴	D ⁵
B.1.1.7	UK	T1001I A1708D I2230T		Q27 Y73C R52I	N501Y A570D P681H T716I S982A D1118H			D3L S235F	11288:9 21765:6 21991:3
B.1.351	South Africa	K1655N			D80A D215G K417N E484K N501Y A701V	P71L		T205I	
P.1	Brazil	S1188L K1795Q	G174C	E92K	L18F T20N P26S D138Y R190S K417T E484K N501Y H655Y T1027I			P80R	11288:9
A.23.1	Uganda				F157L V367F Q613H P681R				
B.1.525	UK, Nigeria	L4715F			E484K Q52R Q677H F888L	L21F I82T			11288:9 21765:6 28278:3
B.1.526^[2]	USA	T226I P861L Q876H L3202P T3953I P4716L Q5413H			L5F T95I D253G E484K D614G A701V			P199L M234I	
B.1.617^[3]	India	T1567I T3646A P4716L G5530C M5753I K6711R S6713A			T95I G142D E154K L452R E484Q D614G P681R Q1071H		I82S	R203M D377Y	

¹ Spike glykoprotein² Envelope protein³ Membrane⁴ N-terminus⁵ Deletion^[2] Based on West et al. 2021^[3] Based on Yadav et al. 2021

References

- [1] Tang, B.; He, F.; Liu, D.; Fang, M.; Wu, Z.; Xu, D. AI-aided design of novel targeted covalent inhibitors against SARS-CoV-2. *bioRxiv*. **2020**.
- [2] West Jr, A.P.; Barnes, C.O.; Yang, Z.; Bjorkman, P.J. SARS-CoV-2 lineage B. 1.526 emerging in the New York region detected by software utility created to query the spike mutational landscape. *bioRxiv*. **2021**.
- [3] Yadav, P.D.; Sapkal, G.N.; Abraham, P.; Ella, R.; Deshpande, G.; Patil, D.Y.; Nyayanit, D.A.; Gupta, N.; Sahay, R.R.; Shete, A.M.; Panda, S.; Bhargava, B.; Mohan, V.K. Neutralization of variant under investigation B. 1.617 with sera of BBV152 vaccinees. *bioRxiv*. **2021**.